processes

MDPI

Article

Selective Recovery of Ce and La from Coal Ash Leachates by Stepwise pH-Controlled Precipitation

Kaster Kamunur [1,2], Olesya Tyumentseva [1], Lyazzat Mussapyrova [1], Aisulu Batkal [1,2], Ardak Karagulanova [1] and Rashid Nadirov [1,2,*]

[1] Institute of Combustion Problems, 172 Bogenbai batyr str., Almaty 050012, Kazakhstan; kamunur.k@mail.ru (K.K.); otyumentseva@knu.kazatomprom.kz (O.T.); lyazzat.mussapyrova@gmail.com (L.M.); abatkalova@mail.ru (A.B.); ardak.karagulanova@gmail.com (A.K.)
[2] Faculty of Chemistry and Chemical Technology, Al-Farabi Kazakh National University, Almaty 050040, Kazakhstan
* Correspondence: nadirov.rashid@gmail.com; Tel.: +7-747-452-05-25

Abstract

Coal ash represents an abundant secondary resource of rare earth elements (REEs), but their recovery is hindered by low concentrations in leachates and the presence of large amounts of competing matrix elements such as Fe, Al, Ca, and Mg. In this study, a stepwise pH-controlled precipitation approach was applied to real sulfuric acid coal ash leachates for selective recovery of Ce and La. The process combined impurity scrubbing, oxidative precipitation of Ce, and phosphate precipitation of La. Nearly complete recovery was achieved, with >95% of both Ce and La recovered and >99% phase purity. Selectivity analysis further demonstrated strong discrimination of REEs over matrix elements, with Ce showing >400 selectivity over Fe, Al, and Ca, and La showing ~170 over the same ions and ~17 over Ce. These results show the efficiency of the approach under realistic multi-element conditions.

Keywords: coal ash; lanthanum; cerium; leachate; pH-controlled precipitation

Received: 6 September 2025
Revised: 6 October 2025
Accepted: 8 October 2025
Published: 9 October 2025

Citation: Kamunur, K.; Tyumentseva, O.; Mussapyrova, L.; Batkal, A.; Karagulanova, A.; Nadirov, R. Selective Recovery of Ce and La from Coal Ash Leachates by Stepwise pH-Controlled Precipitation. *Processes* **2025**, *13*, 3203. https://doi.org/10.3390/pr13103203

1. Introduction

Rare earth elements (REEs) play an important role in modern technologies due to their unique electronic, magnetic, and catalytic properties. They are essential for the manufacturing of permanent magnets, batteries, catalysts, and advanced electronics [1–3]. For instance, experts forecast that demand for permanent-magnet REEs could grow by around 5% annually, spurred by the expansion of electrification and renewable energy systems [4]. Light REEs such as lanthanum (La) and cerium (Ce) are particularly abundant and typically account for approximately 60% of total REE mass in ore and secondary resources, making their effective recovery critically important. Despite abundance, La and Ce recovery from complex matrices (e.g., coal fly ash, phosphogypsum) is hindered by high background levels of matrix elements such as Fe, Al, Ca, and Mg [5].

Coal ash (CA) generated from thermal power plants have emerged as promising secondary resources for REEs recovery, particularly for light REEs. Numerous studies have reported total REE concentrations in CA in the range of 200–500 ppm, depending on the coal origin and combustion conditions [6–8]. Despite this potential, the utilization of coal ash for REE recovery is constrained by several factors. REE concentrations are typically low and vary widely, necessitating pre-concentration or selective leaching strategies. In addition, the

ash matrix is chemically complex, often rich in aluminum, iron, calcium, magnesium, and silicates, which interfere with REE extraction and downstream purification steps [9–12].

Acid leaching remains the most prevalent approach for recovering REEs from CA, with sulfuric [13,14], hydrochloric [15–17], and nitric acids [18,19] as common reagents. While these acids efficiently dissolve REEs, they also extract significant amounts of matrix elements such as aluminum, iron, and calcium, increasing downstream purification challenges. Green reagents, including organic acids [20–22], deep eutectic solvents [23–25], and biogenic leaching agents [26,27], are increasingly explored for REE extraction from coal ash due to their reduced environmental impact and improved safety compared to strong mineral acids; however, they generally provide lower leaching efficiency and slower kinetics.

Among the available methods for coal ash processing, sulfuric acid leaching is the most widely used because of its low cost, high acidity, and good compatibility with industrial practice [13]. It is particularly efficient for transferring light REEs such as La and Ce from the aluminosilicate matrix into solution, with recoveries often exceeding 70–80% under optimized conditions. The main difficulty, however, is not in leaching itself but in the subsequent separation of REEs from the solution. Leachates usually contain large amounts of Fe^{3+}, Al^{3+}, Ca^{2+}, and Mg^{2+}, which hinder selective precipitation and lead to co-precipitation. In addition, the chemical similarity of light REEs, especially between La^{3+} and Ce^{3+}, complicates their separation and requires strict control of downstream conditions.

Several concrete approaches have been developed for selective precipitation of REEs from sulfate leach solutions. Nasar et al. implemented fractional precipitation of REEs from sulfate leach solutions using staged pH adjustment with sodium sulfate and disodium hydrogen phosphate, enabling sequential removal of Fe and Al impurities followed by REE precipitation as double sulfates or hydroxides [28]. Lv and co-authors demonstrated that oxalic acid can be used to selectively precipitate REEs as oxalates from sulfuric leachates, achieving high yields and selectivity, particularly for light REEs [29]. Gomes et al. developed a staged precipitation approach, gradually adding reagents and adjusting physical–chemical conditions to separate REEs from major metals in unpurified leachates, which streamlines purification and recovery [28]. Xing et al. reported a stepwise separation of REEs and Al from coal fly ash using mechanochemical activation and alkaline pre-desilication, with emphasis on the role of interfering ions and their selective removal [30]. Praneeth et al. [31] investigated sorption-assisted precipitation of REEs from fly ash leachates containing competing ions, achieving effective separation of Fe, Al, and REEs. In addition, the paper [32] provided a detailed analysis of the precipitation mechanism of REEs in Fe- and Al-rich solutions, optimizing conditions to improve product purity. Despite notable progress, current methods for REE recovery from CA leachates often lack selectivity and require complex, reagent-intensive steps. In particular, the separation of light REEs such as La and Ce remains difficult due to their chemical similarity and interference from major matrix elements. Phosphate-based stepwise precipitation has received limited attention, especially under realistic leaching conditions.

The novelty of this work lies in the selective stepwise recovery of Ce and La from real coal ash sulfuric leachates that are rich in interfering ions such as Fe, Al, Ca, and Mg. By combining impurity scrubbing with pH-controlled Ce oxidation and subsequent La phosphate precipitation, phase-pure products were obtained with minimal co-precipitation. A complete material balance demonstrated >95% recovery of both elements, underscoring the practical relevance of the approach under realistic leaching conditions. This study proposes a pH-controlled precipitation strategy guided by thermodynamic modeling, enabling sequential removal of matrix impurities and selective recovery of cerium and lanthanum. The approach is validated using real sulfate leachates from CA, with material balance confirming its effectiveness and selectivity.

2. Materials and Methods

2.1. Materials and Reagents

Coal ash sample for leaching was collected from ash deposit of Almaty combined heat and power plant (CHPP)—2 (Kazakhstan).

All reagents used were of analytical grade. Cerium nitrate hexahydrate ($Ce(NO_3)_3 \cdot 6H_2O$, 99.99%), lanthanum nitrate hexahydrate ($La(NO_3)_3 \cdot 6H_2O$, 99.99%), aluminum sulfate ($Al_2(SO_4)_3 \cdot 18H_2O$), ferric sulfate ($Fe_2(SO_4)_3 \cdot xH_2O$), calcium sulfate dihydrate ($CaSO_4 \cdot 2H_2O$), magnesium sulfate heptahydrate ($MgSO_4 \cdot 7H_2O$), orthophosphoric acid (H_3PO_4, 85%), and hydrogen peroxide (H_2O_2, 30%) were purchased from Aladdin Biochemical Technology Co., Ltd. (Shanghai, China). Sulfuric acid (H_2SO_4) and sodium hydroxide (NaOH) were obtained from Reactivsnab LLP (Almaty, Kazakhstan). Distilled water was used throughout all experiments.

2.2. Preparation of Real Leachate

To simulate leaching conditions for coal ash, a batch of 1000 g of coal ash was treated with 10 L of 1 M H_2SO_4 at 80 °C for 4 h, using a solid-to-liquid ratio of 1:10 (w/v) under continuous stirring. The leaching parameters were selected based on preliminary optimization trials. The slurry was cooled to room temperature, filtered through vacuum filtration, and the clear leachate was collected. The solution was analyzed by ICP-OES to determine the concentrations of Ce, La, Al, Fe, Ca, and Mg (Table 1), and used as the reference for synthetic model formulation.

Table 1. Chemical composition of the real leachate obtained after sulfuric acid leaching of coal ash (100 g ash in 1 L of 1 M H_2SO_4, 80 °C, 4 h).

Al, mg/L	Fe, mg/L	Ca, mg/L	Mg, mg/L	P, mg/L	Na+K, mg/L	Si, mg/L	Ce, mg/L	La, mg/L
11,977	4320	850	514	117	149	64	4.77	1.81

2.3. Preparation of Model Leachate

Based on the elemental composition of the real leachate, model solutions were prepared by dissolving appropriate quantities of $Ce(NO_3)_3$, $La(NO_3)_3$, $Fe_2(SO_4)_3$, $Al_2(SO_4)_3$, $CaSO_4$, and $MgSO_4$ in deionized water. The final concentrations of metal ions were adjusted to match the real leachate, with Ce and La at 4.77 mg/L and 1.81 mg/L, respectively. The pH was maintained at ~1.7 using diluted sulfuric acid to simulate the acidic conditions of the real system.

2.4. Precipitation of Metals

To establish optimal conditions for the removal of interfering matrix elements, a series of pH-controlled precipitation experiments were conducted using a synthetic sulfate leachate. The pH was gradually adjusted by the dropwise addition of 1 M NaOH under constant stirring at room temperature. For each pH point, aliquots were withdrawn after 30 min of equilibration and filtered. The concentrations of dissolved Fe, Al, Ca, Mg, la, and Ce in the filtrates were determined by ICP-OES.

A series of stepwise precipitation experiments was performed across a range of pH values and reagent dosages, with the aim of selectively separating Fe, Al, Ca, Mg, Ce, and La. The conditions for individual precipitation steps were gradually optimized based on solubility diagrams (Section 3.1).

In the case of selective precipitation of Ce, Ce^{3+} oxidation was induced by adding 30% H_2O_2 into leachate, which ensured the conversion of Ce^{3+} to Ce^{4+}.

2.5. Characterization of Liquid and Solid Samples

Elemental concentrations in solution were determined using inductively coupled plasma optical emission spectrometry (ICP-OES; Optima 8300, PerkinElmer, Waltham, MA, USA). Each measurement was performed in triplicate, with relative standard deviations not exceeding ±3%. Solid precipitates were washed with distilled water, dried at 60 °C, and characterized by X-ray diffraction (XRD; DW-27 Mini, Dandong Dongfang, Dandong, China) and Fourier-transform infrared spectroscopy (FTIR; InfraLUM FT-08, Lumex, St. Petersburg, Russia, 3800–600 cm^{-1}). To determine the elemental composition of solids, the samples were subjected to microwave-assisted acid digestion, and the resulting solutions were analyzed by ICP-OES. Thermogravimetric and differential scanning calorimetry (TG–DSC) analyses were conducted using a BXT-TGA 103 analyzer (Baixi Instrument Technology Co., Shanghai, China). Scanning electron microscopy (SEM) and surface elemental analysis were performed using a JEOL JSM-6490LA microscope equipped with a JED-2300 energy-dispersive X-ray spectroscopy (EDS) system (JEOL Ltd., Tokyo, Japan).

3. Results and Discussion

3.1. Thermodynamic Modeling and Precipitation Strategy

In the recovery of REEs from coal fly ash leachates, one of the key challenges is the selective removal of interfering major elements such as calcium, aluminum, iron, and magnesium. These matrix components not only consume reagents during downstream processing but may also coprecipitate with REEs or form unwanted by-products [33]. Therefore, a rational separation strategy must first ensure the effective removal of such interfering species, followed by the controlled recovery of target REEs, primarily lanthanum and Ce in this case. To design such a multistep separation protocol, it is essential to determine the pH domains in which each element can be selectively removed. For this purpose, we constructed a thermodynamic solubility diagram based on experimentally established solubility product constants (Ksp) and phosphate speciation equilibria. This diagram aims to identify pH regions where selective precipitation of iron, aluminum, calcium, and magnesium is thermodynamically favored, without significant losses of REEs, and subsequently, to define the optimal pH window for the selective precipitation of lanthanum and Ce. The diagram was constructed at 25 °C using the following assumptions. Hydroxide solubilities of $Fe(OH)_3$, $Al(OH)_3$, and $Mg(OH)_2$ were modeled based on their solubility product constants (Ksp) using the mass-action expression $\log[M^{n+}] = \log Ksp - n \cdot \log[OH^-]$, where $[OH^-] = 10^{-14}/[H^+]$. Calcium was considered separately, as it predominantly forms calcium sulfate ($CaSO_4 \cdot 2H_2O$) in sulfate-rich media; its solubility was estimated assuming a fixed sulfate concentration of 0.5 mol/L, reflecting the conditions of sulfuric acid leaching, consistent with measured gypsum solubility in $CaSO_4$–H_2SO_4–H_2O systems [34]. For La and Ce, precipitation was modeled as phosphate-driven, using the equilibrium $MPO_4(s) + H^+ \rightleftharpoons M^{3+} + HPO_4^{2-}$, leading to $\log[Ln^{3+}] = \log Ksp - pH + pKa_3 - \log[HPO_4^{2-}]$ (here, M denotes La and Ce). Phosphate speciation was calculated from the dissociation constants of phosphoric acid ($pKa_1 = 2.15$, $pKa_2 = 7.20$, $pKa_3 = 12.35$), assuming a total phosphate dose of 50 mM [35–37]. The model did not account for complexation, activity coefficients, or redox equilibria, and is therefore considered a first-order approximation. The resulting solubility profiles (Figure 1) show that iron precipitates first as $Fe(OH)_3$ at pH $\gtrsim$ 1.5–2.0, followed by aluminum at pH $\gtrsim$ 3.0–4.0.

Calcium is primarily controlled by $CaSO_4$ solubility, limiting its free ion concentration even in acidic solutions, while magnesium remains highly soluble throughout the acidic range. In the presence of phosphate, lanthanum and Ce begin to precipitate as REE phosphates at pH ≈ 2.5–3.5, with Ce phosphate forming slightly earlier than lanthanum phosphate due to its lower solubility. This behavior enables the design of a rational three-

stage precipitation scheme: (1) Fe-scrub stage (pH ≈ 1.5–2.0) for selective removal of iron as $Fe(OH)_3$; (2) Al-scrub stage (pH ≈ 3.0–4.0) for removal of residual aluminum with limited co-removal of Ca (as gypsum) and Mg, while REEs remain in solution; (3) REE precipitation stage: after Al removal, the solution should be adjusted to pH 2.5–3.2 and dosed with H_3PO_4; when required, Ce^{3+} should be selectively oxidized to Ce^{4+} with H_2O_2 to precipitate Ce (as $CeO_2/Ce(OH)_4$ or $CePO_4$) prior to $LaPO_4$ formation.

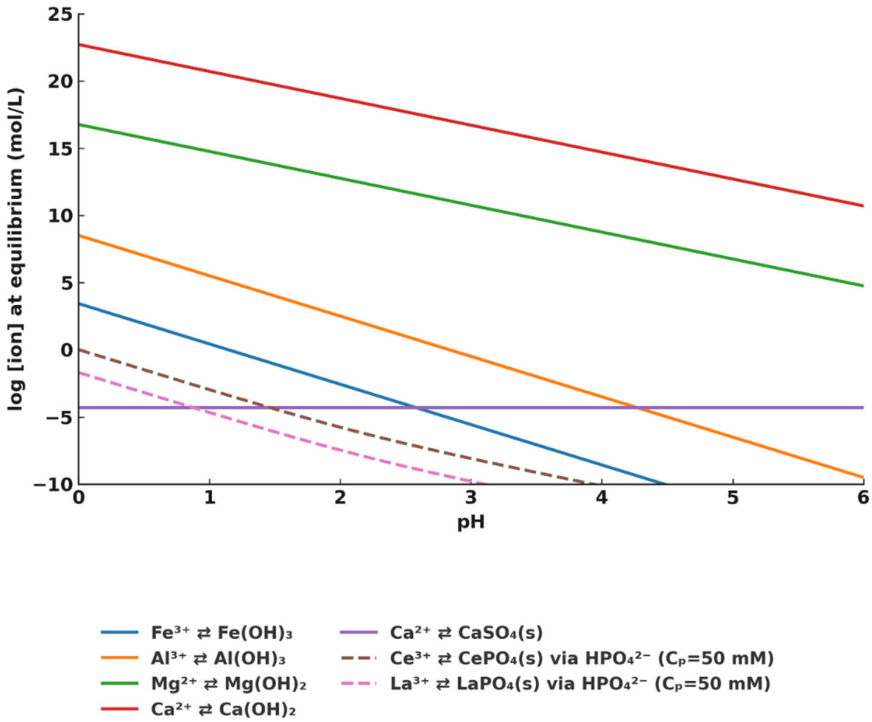

Figure 1. Simplified solubility diagram for key metal species ($Fe(OH)_3$, $Al(OH)_3$, $CaSO_4$, $Mg(OH)_2$, $CePO_4{\cdot}H_2O$, $LaPO_4{\cdot}H_2O$) as a function of pH at 25 °C, calculated based on standard Ksp values. Curves for $CePO_4$ and $LaPO_4$ were computed assuming a total phosphate concentration of 50 mM; the model neglects activity coefficients, complexation, and redox equilibria.

3.2. Precipitation Behavior of Interfering Elements

Figure 2 shows the residual concentrations of Fe, Al, Ca, and Mg in the solution as a function of pH.

The sharp decline of Fe at pH ≈ 1.8–2.0 reflects rapid Fe(III) hydrolysis and precipitation of amorphous $Fe(OH)_3$ governed by its extremely low solubility (Ksp ~10^{-38}), consistent with established hydrolysis/solubility constants of Fe(III) [38]. Al remains largely soluble below pH ≈ 3 and decreases steeply in the pH ≈ 3.0–4.2 window as $Al(OH)_3$ forms (Ksp ~10^{-32}–10^{-34}), in agreement with Ksp-based predictions; the higher onset than Fe is due to weaker hydrolysis of Al at low pH. Ca shows a gradual drop toward a sulfate-controlled plateau because its activity is limited by equilibrium with gypsum/anhydrite ($CaSO_4{\cdot}2H_2O/CaSO_4$); at fixed [$SO_4^{2-}$] typical of sulfuric leachates, dissolved Ca approaches the $CaSO_4$ solubility (order 10^{-2} M total $CaSO_4$ in pure water at 25 °C), and the smoothed curve reflects nucleation/kinetic effects rather than pH control. Mg remains nearly unchanged across pH 1–5 because brucite formation requires much higher [OH^-] ($Ksp(Mg(OH)_2) \approx 5.6 \times 10^{-12}$), so precipitation is thermodynamically unfavorable in the acidic region. These trends are consistent with experimental data on the selective precipitation of Fe/Al from acidic process solutions; Fe is removed at lower pH, whereas effective Al precipitation requires higher pH, as confirmed by hydrometallurgical studies [39].

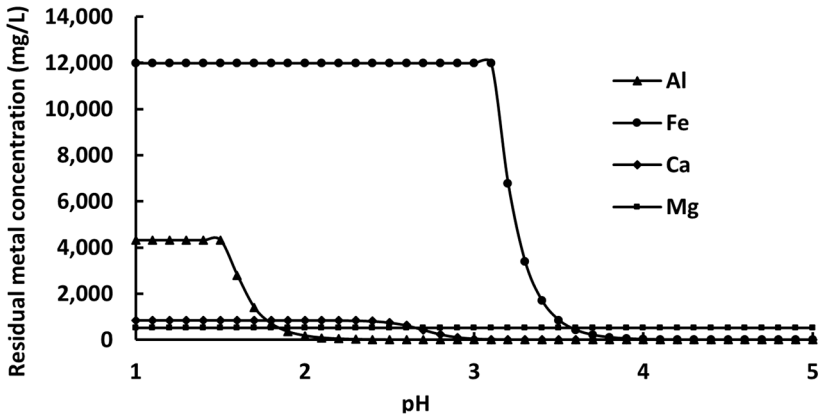

Figure 2. Residual concentrations of Fe, Al, Ca, and Mg in the solution as a function of pH.

Figure 3 shows the XRD patterns of the precipitates formed during the sequential removal of major interfering elements. The pattern in Figure 3a corresponds to the solid phase obtained at pH ≈ 2.0–2.2, while Figure 3b represents the precipitate collected at pH ≈ 4.0–4.2 after further pH adjustment.

At pH ≈ 2.0–2.2 (Figure 3a), the precipitate primarily consisted of gypsum ($CaSO_4 \cdot 2H_2O$) and goethite (α-FeOOH), along with residual silica (SiO_2) derived from the ash matrix. These phases reflect the early-stage removal of calcium and iron under low-pH conditions. At pH ≈ 4.0–4.2 (Figure 3b), additional crystalline phases were detected, including natrojarosite ($NaFe_3(SO_4)_2(OH)_6$) and alunite ($KAl_3(SO_4)_2(OH)_6$). These basic sulfates indicate the progressive hydrolysis of iron and aluminum in sulfate media during the second precipitation step. The formation of these stable sulfate-bearing phases under acidic conditions is consistent with the expected behavior of Fe^{3+} and Al^{3+} in the presence of Na^+, K^+, and SO_4^{2-} ions.

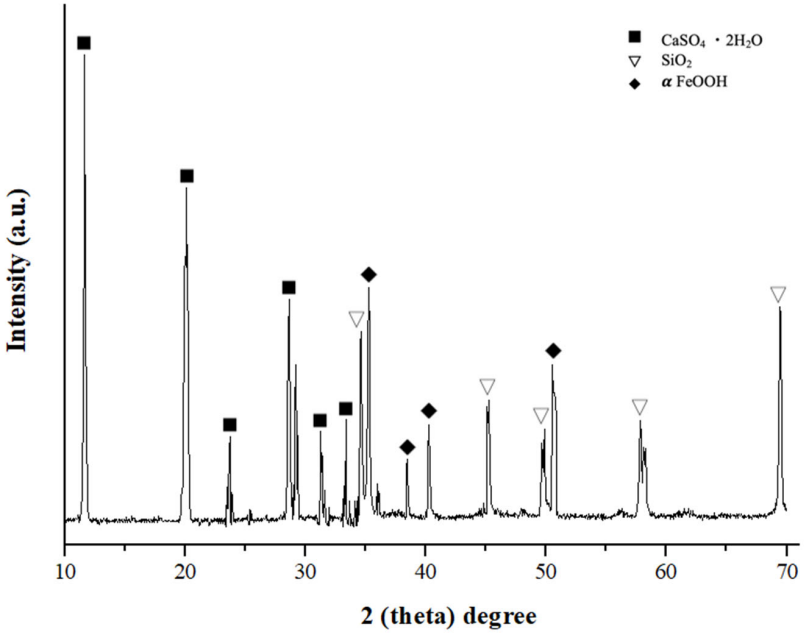

(**a**)

Figure 3. *Cont.*

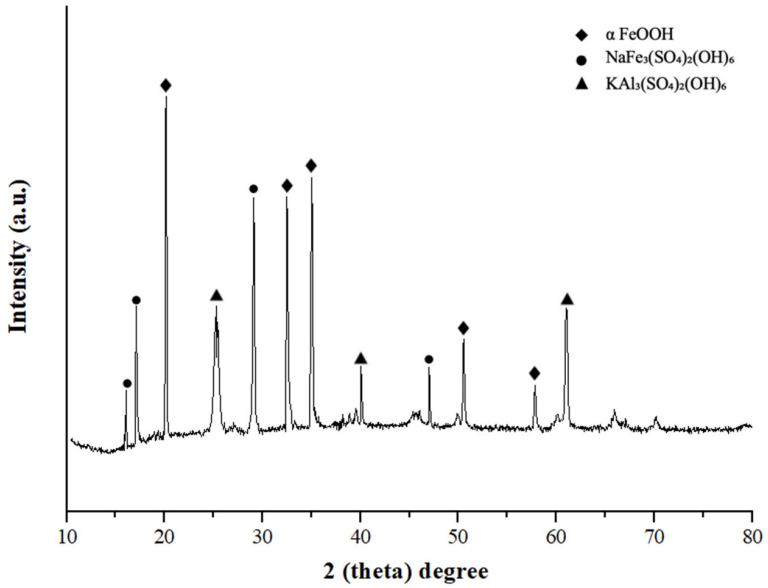

(**b**)

Figure 3. XRD pattern of the precipitate obtained at pH ≈ 2.0–2.2 (**a**) and pH ≈ 4.0–4.2 (**b**).

Thus, increasing the solution pH to approximately 4.2–4.3 was found to be sufficient to minimize the concentrations of major interfering species (Fe, Al, Ca) without the need for further neutralization. This pH was selected as the endpoint of the impurity removal stage. After this stage, a solution of the following composition was obtained, mg/L: Fe < 0.01, Al 0.03, Ca 1.92, Mg 511, La 4.75, Ce 1.79.

Under these conditions, La and Ce remained at their initial concentrations because, in the acidic sulfate leachate (pH 1–5), trivalent REE ions are thermodynamically stable and their hydroxides do not reach supersaturation ($Ln(OH)_3$ precipitation requires pH $\gtrsim$ 7–8); additionally, Ce remained reduced as Ce^{3+} (no oxidant was applied), preventing formation of insoluble Ce(IV) phases, and the high ionic strength/sulfate complexation contributed to stabilizing the dissolved REE species.

3.3. Precipitation of La and Ce from the Purified Leachate

As shown in the previous section, the pH of the purified leachate was approximately 4.2–4.3, which is above the solubility limit of REE phosphates in the presence of phosphate. The purified sulfate leachate was first acidified to pH 2.0–2.2 using 1 M H_2SO_4. Orthophosphoric acid was then added to reach a total phosphate concentration of 50 mM. Under constant stirring, the pH of the solution was gradually increased to 3.4–3.5 with 1 M NaOH ($\leq$0.5 mL/min). The suspension was aged for 60 min at the set pH, then filtered through a 0.45 μm PES membrane. The solids were washed with distilled water and dried at 60 °C.

The precipitation behavior of Ce and La was evaluated in the presence of phosphate over a pH range of 2.0 to 3.5, with and without oxidative pretreatment. Residual concentrations of both elements were monitored by ICP-OES (Figure 4).

To illustrate the separation behavior, the recovery percentages of Ce, La, and major competing ions (Fe, Al, Ca, Mg) were plotted as a function of pH (Figure 5).

To quantify the degree of separation, selectivity coefficients were calculated as the ratio of distribution coefficients of REEs to those of major competing ions. At the Ce precipitation step (pH ≈ 2.7–2.8), the selectivity of Ce over Fe, Al, and Ca exceeded 400, that confirms nearly exclusive removal of Ce with negligible co-precipitation of matrix elements. During the La precipitation step (pH ≈ 3.4–3.5), the selectivity of La over Fe,

Al, and Ca was ~170, while the selectivity of La over Ce was lower (~17), that reflects minor co-precipitation of Ce with La phosphate. These values show the high efficiency and selectivity of the stepwise precipitation strategy.The observed precipitation sequence can be rationalized in terms of hydrolysis equilibria and solubility products. Iron(III) and aluminum(III) hydrolyze strongly in acidic sulfate media, with solubility products of $Fe(OH)_3$ (Ksp $\approx 10^{-38}$) [40] and $Al(OH)_3$ (Ksp $\approx 10^{-33}$–10^{-34}) [41], that explains their removal at pH $\approx$ 2 and $\approx$ 3–4, respectively. In contrast, Ca and Mg remain soluble in this range due to much higher hydroxide solubility ($Ksp(Ca(OH)_2) \approx 7.9 \times 10^{-6}$ [42]; $Ksp(Mg(OH)_2) \approx 1.2 \times 10^{-12}$ [43]). For rare earths, hydrolysis is weak in strongly acidic sulfate solutions, but the addition of phosphate promotes precipitation through the very low solubility of REE phosphates. Reported solubility products decrease from heavy to light REEs, e.g., log $Ksp(LaPO_4 \cdot H_2O) \approx -25.6$, log $Ksp(CePO_4 \cdot H_2O) \approx -26.0$) [44].

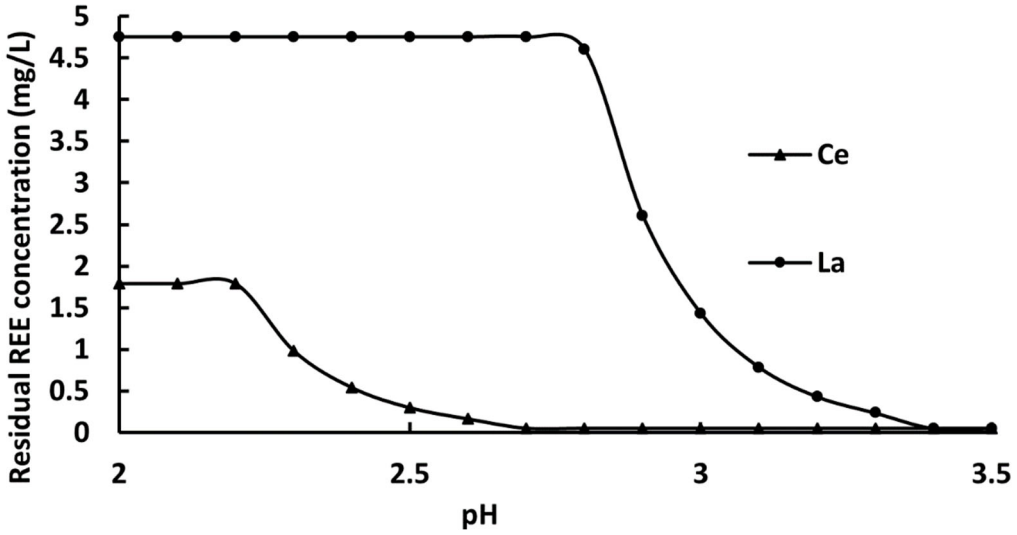

Figure 4. Residual concentrations of Ce and La as a function of pH during phosphate-induced precipitation from the purified sulfate leachate.

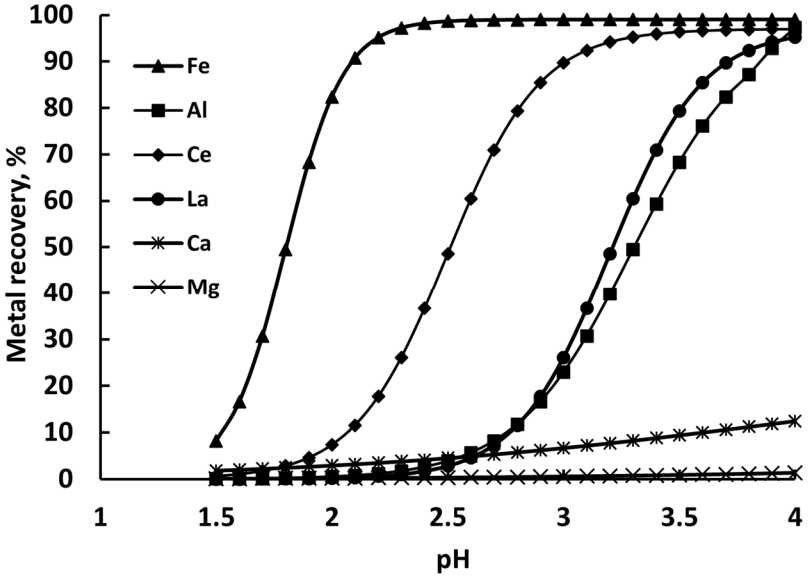

Figure 5. Recovery of Ce, La, and major competing ions (Fe, Al, Ca, Mg) as a function of pH during stepwise precipitation from coal ash leachate.

Ce began to precipitate at pH $\approx$ 2.2, with more than 97% removal achieved by pH 2.7. In contrast, La precipitation initiated above pH 2.8 and reached similar removal efficiency

only near pH 3.4. This difference in precipitation onset provides a thermodynamic basis for potential stepwise separation of Ce and La via controlled pH adjustment. Residual concentrations of both REEs decreased with increasing pH but plateaued at approximately 0.05 mg/L, which reflects both the equilibrium solubility of REE phosphates under the given conditions and the detection limits of ICP-OES analysis.

Upon reaching pH ≈ 3.4–3.5, a precipitate of the following composition was obtained, wt. %: La 22.1%, Ce 8.4%, P 11.2%, Al < 0.05, Fe < 0.01, Ca 0.2. To evaluate the effect of thermal treatment, the dried precipitate was calcined at 700 °C for 3 h in air. After calcination, the solid was re-analyzed by elemental analysis to assess compositional changes. The resulting calcined material contained: La—25.9%, Ce—9.8%, P—13.1%, Ca—0.21%, Al—<0.05, Fe—<0.01.

To separate La and Ce, the precipitation was carried out in two steps.

(1) Cerium step. The pH was adjusted to 2.7–2.8 with 1 M NaOH added dropwise (≤1 mL/min) at 25 ± 2 °C under stirring at 400 rpm. No phosphate was added at this point. A single dose of 30% H_2O_2 was introduced in ~1000-fold molar excess relative to the dissolved Ce. The suspension was stirred for 30 min while maintaining the pH within 2.7–2.8, followed by an additional 30 min of aging; a persistent pale-yellow coloration indicated oxidation of Ce^{3+} to Ce^{4+}. The precipitate was separated by filtration, washed with 0.01 M H_2SO_4 and distilled water, and dried at 60 °C.

(2) Lanthanum step. The filtrate obtained after Ce removal was (optionally) re-acidified to pH 2.0–2.2 to standardize the starting conditions. Orthophosphoric acid was then added to achieve a total phosphate concentration of 25–50 mM. The pH was gradually raised to 3.4–3.5 using 1 M NaOH (≤0.5 mL/min) over 30–60 min while stirring at 25 ± 2 °C and 400 rpm. The suspension was held at this pH for 60 min to complete precipitation, with pH stability verified, after which the solid was collected by filtration, washed with distilled water, and dried at 60 °C.

The corresponding XRD patterns are shown in Figure 6a,b.

At pH ≈ 2.7–2.8 (Figure 6a), the diffraction pattern showed well-defined peaks corresponding to CeO_2, indicating that cerium was selectively recovered in oxide form during the first precipitation step. The absence of hydrated phases is attributed to the oxidation of Ce^{3+} to Ce^{4+} under the applied conditions, which favors the formation of the thermodynamically stable oxide rather than hydrated phosphate species. In contrast, the subsequent precipitate formed at pH ≈ 3.4–3.5 (Figure 6b) exhibited diffraction reflections characteristic of $LaPO_4 \cdot H_2O$, consistent with the expected lanthanum phosphate hydrate.

To elucidate the thermal behavior and phase evolution of the precipitate, thermogravimetric analysis coupled with differential scanning calorimetry (TGA–DSC) was conducted in air from 25 to 800 °C. The results are shown in Figure 7.

The TG curve reveals a total mass loss of approximately 11.1% in three distinct steps. The initial weight loss (~6.5%) below 230 °C corresponds to the removal of physically adsorbed and weakly bound water. The second stage (~3.1%) between 300 and 500 °C is attributed to the dehydration of $LaPO_4 \cdot H_2O$, resulting in the formation of anhydrous $LaPO_4$. This conversion is accompanied by a broad endothermic peak on the curve. A minor thermal event observed around 650–700 °C may be related to structural rearrangement or recrystallization of phosphate phases. No significant mass change is observed beyond 750 °C, that indicates the thermal stability of the final REE-containing phases.

Figure 8 shows the diffraction pattern of the product obtained by calcination (≈650 °C) of the $LaPO_4$ H_2O precipitate.

The XRD pattern of the calcined product shows sharp reflections of monazite-type $LaPO_4$, with the most intense peaks at 2θ ≈ 26.0°, 28.1°, 29.0°, and 48.6°. In comparison with the diffractogram of $LaPO_4 \cdot H_2O$ (Figure 6b), the peaks are narrower and no low-angle

features associated with structural water are observed, confirming dehydration and the formation of crystalline anhydrous $LaPO_4$.

Figure 9 shows SEM images of the obtained solids with (a) bulk precipitate formed by non-stepwise REE precipitation, (b) selective Ce precipitate at pH ≈ 2.7–2.8, (c) selective La precipitate in the form of $LaPO_4 \cdot H_2O$ at pH ≈ 3.4–3.5 and (d) calcined La phosphate after dehydration.

Figure 9a reveals irregular, loosely aggregated particles with heterogeneous morphology, typical of the non-stepwise precipitation of REEs. In Figure 9b, elongated and faceted crystallites are observed, corresponding to the Ce-rich product selectively precipitated at pH ≈ 2.7–2.8. The structure shown in Figure 9c consists of dense, block-like particles with smoother surfaces, characteristic of the La-rich hydrate formed at pH ≈ 3.4–3.5. Figure 9d exhibits a compact fine-grained texture, resulting from the thermal transformation of the La phosphate into monazite-type $LaPO_4$.

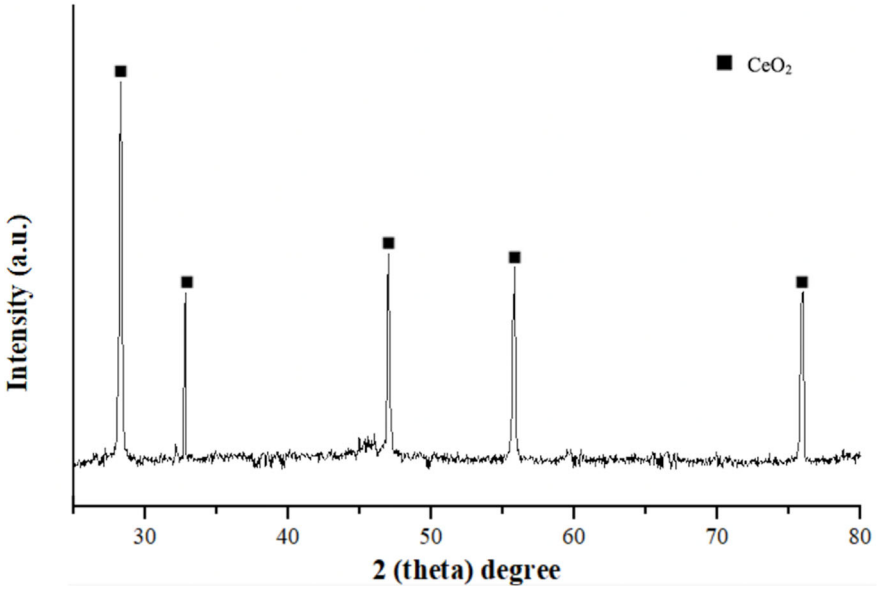

(**a**)

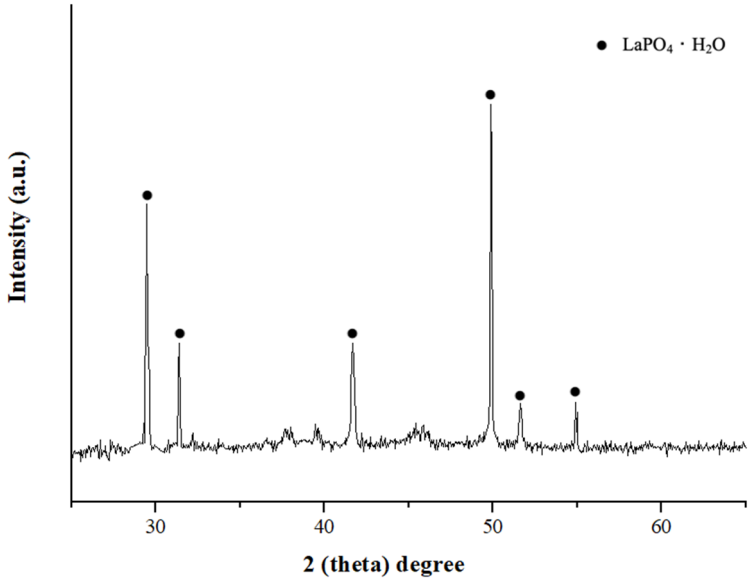

(**b**)

Figure 6. XRD patterns of precipitates at pH ≈ 2.7–2.8 (**a**) and ≈ 3.4–3.5 (**b**).

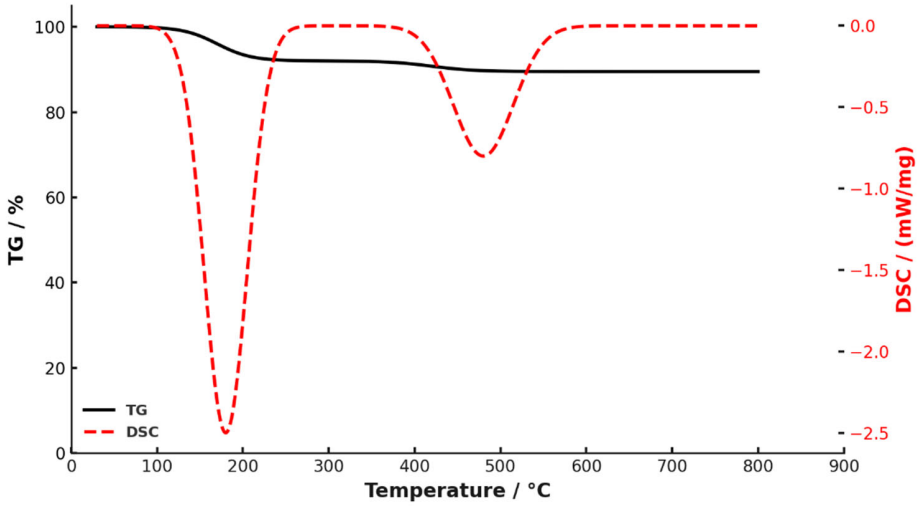

Figure 7. TGA–DSC curves of the precipitate recorded in air from 25 to 800 °C.

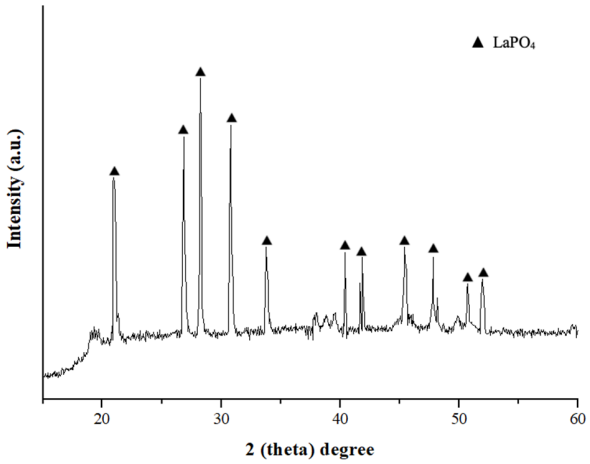

Figure 8. XRD pattern of the product obtained by calcination (≈650 °C) of the $LaPO_4 \cdot H_2O$ precipitate.

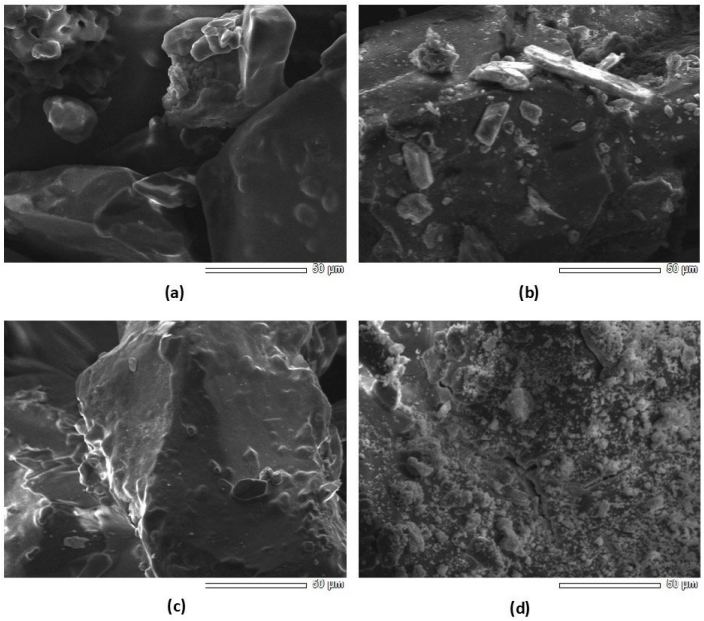

Figure 9. SEM images of REE precipitates: (**a**) non-stepwise precipitation, (**b**) selective Ce precipitation, (**c**) selective La precipitation as hydrate, (**d**) calcined La phosphate.

Thus, a stepwise pH-controlled precipitation strategy allows efficient separation of Ce and La from sulfate leachates. Ce is selectively recovered as crystalline CeO_2 at lower pH, while lanthanum precipitates as $LaPO_4 \cdot H_2O$ at higher pH. Subsequent thermal treatment converts the hydrate into stable monazite-type $LaPO_4$. The combined precipitation–calcination approach provides a rational route for obtaining phase-pure REE products.

3.4. Material Balance and Metals Distribution

To quantitatively assess the efficiency and selectivity of the developed precipitation strategy, a complete material balance was established. The balance was constructed on a basis of 1 L of sulfuric leachate obtained from 100 g of coal ash. The following notation was adopted: S0—initial leachate after sulfuric acid leaching, P1—solid phase obtained after Fe-scrub (pH ≈ 1.5–2.0), S1—filtrate after P1, P2—solid phase obtained after Al-scrub (pH ≈ 3.0–4.2), S2—purified leachate, P3—Ce-rich precipitate formed at pH 2.7–2.8, S3—filtrate after P3, P4—La-rich precipitate formed at pH 3.4–3.5, S4—final raffinate.

In Table 2 the material balance of the major matrix components and the target REEs during the purification stages is presented.

Table 2. Material balance of major and target elements during impurity removal (for 1 L of initial leachate).

Stream	Al, mg	Fe, mg	Ca, mg	Mg, mg	Si, mg	Ce, mg	La, mg
S0	11,977.00	4320.00	850.00	514.00	64.0	4.77	1.81
P1	598.85	4233.60	833.00	1.54	14.3	-	-
S1	11,378.15	86.40	17.00	512.46	49.4	4.77	1.81
P2	11,378.12	86.39	15.08	1.46	10.1	-	-
S2	0.03	0.01	1.92	511.00	38.9	4.77	1.81

The initial sulfuric leachate (S0) contained high concentrations of Al, Fe, and Ca, along with Mg and trace amounts of Ce and La. During the Fe-scrub step (P1), more than 98% of Fe was removed, accompanied by extensive co-precipitation of Ca. Aluminum was only slightly reduced at this stage. In the subsequent Al-scrub (P2), Al was almost completely eliminated (>99.9%), together with the residual Fe, while Mg largely remained in solution. Of the initial 64.0 mg of Si present in the leachate, 14.3 mg was removed during Fe precipitation (P1), and 10.1 mg during Al precipitation (P2). As a result, the purified solution (S2) retained Ce and La quantitatively, while approximately 39 mg of dissolved Si remained.

Table 3 presents the material balance during the two-step REE precipitation.

Table 3. Material balance of major and target elements during two-step REE precipitation (for 1 L of initial leachate).

Stream	Ce, mg	La, mg	Ca, mg	Si, mg	Mg, mg	Al, mg	Fe, mg
S2	4.77	1.81	1.92	38.2	511.00	0.03	0.01
P3	4.50	-	<0.01	-	-	<0.01	-
S3	0.20	1.81	1.92	38.2	511.00	0.03	0.01
P4	0.10	1.70	0.01	-	0.00	<0.01	<0.01
S4	0.05	0.05	1.90	38.2	510.50	0.02	0.01

The purified leachate (S2) contained 4.77 mg Ce and 1.81 mg, together with residual amounts of Ca, Mg, Al, and Fe. At the first precipitation step (P3, pH ≈ 2.7–2.8), about 4.50 mg of Ce was selectively removed as CeO_2, while La remained entirely in solution. In the second step (P4, pH ≈ 3.4–3.5), La was almost completely precipitated (1.70 mg) as $LaPO_4 \cdot H_2O$, together with a minor fraction of Ce as $CePO_4 \cdot H_2O$. Si, however, did not precipitate under these conditions and remained fully in the final raffinate. This was expected, as the absence of Fe and Al precluded the formation of siliceous flocs, and the neutral molecular form of silica exhibits minimal affinity for phosphate or lanthanum surfaces at this pH The final raffinate (S4) contained only ≈0.05 mg of each REE, confirming near-complete recovery. Compared with solvent extraction and ion exchange, which can achieve very high purity but require complex multi-stage circuits and costly reagents, the present stepwise precipitation route provides a simpler option for producing intermediate REE concentrates. In this study, recovery of Ce and La exceeded 95% with phase purity above 99%, achieved directly from real coal ash leachates using only mineral acids and oxidants. Although not a substitute for advanced refining, this approach can serve as a low-cost preparatory step prior to downstream processing.

Although the developed strategy ensures high recovery of Ce and La, their initial concentrations in the leachate (4.77 and 1.81 mg/L, respectively) are low for industrial application. To improve process efficiency, a pre-concentration step (e.g., evaporation, membrane separation, or sorption) could be applied before precipitation. A 10-fold concentration would raise REE levels to ~48 and ~18 mg/L, reducing reagent use and liquid streams. While not tested here, this option is noted as a key consideration for scale-up.

A detailed breakdown of elemental distributions in the solid phases obtained during the two-step REE precipitation is provided in Table 4.

Table 4. Mass balance of metals in precipitates obtained during two-step REE precipitation (for 1 L of initial leachate).

Precipitate	Solid, mg	Ce	La	Ca	Al	Fe
P3	5.50	4.50	-	<0.01	<0.01	<0.01
P4	3.20	0.10	1.70	0.01	0.01	0.01
Closure	-	0.15	0.06	0.02	<0.01	<0.01

In the first precipitate (P3), 5.50 mg of solids were formed, containing 4.50 mg of Ce and only trace amounts of other elements (<0.01 mg). The second precipitate (P4) accounted for 3.20 mg of solids, including 0.10 mg of Ce, 1.70 mg of La, and minor quantities of Ca, Al, and Fe (≈0.01 mg each). Such trace-level impurities are acceptable for intermediate REE concentrates and do not limit their applicability as precursors for commercial separation and refining processes. The results consistently show that the developed scheme ensures efficient removal of impurities and selective recovery of REEs. The small deviations indicated in the closure rows (2–4%) can be attributed to experimental losses during filtration and analytical uncertainty.

4. Conclusions

A stepwise precipitation strategy was developed for the selective separation and recovery of Ce and La from sulfuric acid leachates of coal ash. The approach was guided by thermodynamic modeling and involved sequential removal of matrix impurities (Fe, Al, Ca, Mg), followed by controlled pH adjustment and phosphate addition to induce rare earth precipitation. Fe and Al were effectively removed by hydrolysis at moderately acidic pH levels, while Ce was selectively precipitated as CeO_2 under mildly acidic condi-

tions after oxidative pretreatment. La was subsequently recovered as hydrated phosphate ($LaPO_4 \cdot H_2O$) at higher pH. Thermal treatment of the La precipitate yielded phase-pure, crystalline $LaPO_4$ with a monazite-type structure. SEM analysis revealed distinct morphologies corresponding to different precipitation modes, confirming the effectiveness of the stepwise separation. A complete material balance demonstrated high recovery yields for both REEs and minimal co-precipitation of matrix elements, with mass closure deviations within acceptable limits (2–4%). The proposed method offers an efficient and scalable route for light REE recovery from coal-derived leachates, without the need for organic extractants or harsh processing conditions.

Despite these promising results, the method has certain limitations, including the relatively low initial REE concentrations in coal ash leachates and the need for further optimization of reagent consumption and process integration at larger scale. Nevertheless, the ability to obtain REE-rich concentrates directly from coal combustion residues has important industrial and environmental implications. These outcomes align with the United Nations Sustainable Development Goals, particularly SDG 9 (Industry, innovation, and infrastructure) and SDG 12 (Responsible consumption and production).

Author Contributions: Conceptualization, R.N. and K.K.; methodology, L.M. and O.T.; investigation, L.M., O.T., and A.B.; resources, R.N.; writing—original draft preparation, K.K., O.T., L.M., and A.B.; writing—review and editing, R.N., L.M., and A.K.; validation—A.K. and O.T.; project administration, R.N. All authors have read and agreed to the published version of the manuscript.

Funding: This research was funded by the Science Committee of the Ministry of Science and Higher Education of the Republic of Kazakhstan (Grant no. BR21882017).

Data Availability Statement: The data supporting the results can be made available from the corresponding author upon request.

Conflicts of Interest: The authors declare no conflicts of interest.

References

1. Hossain, M.K.; Hossain, S.; Ahmed, M.H.; Khan, M.I.; Haque, N.; Raihan, G.A. A review on optical applications, prospects, and challenges of rare-earth oxides. *ACS Appl. Electron. Mater.* **2021**, *3*, 3715–3746. [CrossRef]
2. Filho, W.L.; Kotter, R.; Özuyar, P.G.; Abubakar, I.R.; Eustachio, J.H.P.P.; Matandirotya, N.R. Understanding rare earth elements as critical raw materials. *Sustainability* **2023**, *15*, 1919. [CrossRef]
3. Balaram, V. Potential future alternative resources for rare earth elements: Opportunities and challenges. *Minerals* **2023**, *13*, 425. [CrossRef]
4. Gkika, D.A.; Chalaris, M.; Kyzas, G.Z. Review of methods for obtaining rare earth elements from recycling and their impact on the environment and human health. *Processes* **2024**, *12*, 1235. [CrossRef]
5. Wang, S.; Huang, W.; Ao, W. The Distribution of Rare Earth Elements in Coal Fly Ash Determined by LA-ICP-MS and Implications for Its Economic Significance. *Sustainability* **2025**, *17*, 275. [CrossRef]
6. Talan, D.; Huang, Q. A review study of rare Earth, Cobalt, Lithium, and Manganese in Coal-based sources and process development for their recovery. *Miner. Eng.* **2022**, *189*, 107897. [CrossRef]
7. Thomas, B.S.; Dimitriadis, P.; Kundu, C.; Vuppaladadiyam, S.S.V.; Raman, R.S.; Bhattacharya, S. Extraction and separation of rare earth elements from coal and coal fly ash: A review on fundamental understanding and on-going engineering advancements. *J. Environ. Chem. Eng.* **2024**, *12*, 112769. [CrossRef]
8. Agrawal, R.; Ragauskas, A.J. Sustainable recovery of Rare Earth Elements (REEs) from coal and coal ash through urban mining: A Nature Based Solution (NBS) for circular economy. *J. Environ. Manag.* **2025**, *384*, 125411. [CrossRef]
9. Zhang, L.; Chen, H.; Pan, J.; Yang, F.; Long, X.; Yang, Y.; Zhou, C. Rare earth elements recovery and mechanisms from coal fly ash by column leaching using citric acid. *Sep. Purif. Technol.* **2025**, *353*, 128471. [CrossRef]
10. Nadirov, R.; Kamunur, K.; Mussapyrova, L.; Batkal, A.; Tyumentseva, O.; Karagulanova, A. Integrated Compositional Modeling and Machine Learning Analysis of REE-Bearing Coal Ash from a Weathered Dumpsite. *Minerals* **2025**, *15*, 734. [CrossRef]
11. Palozzi, J.; Bailey, J.G.; Tran, Q.A.; Stanger, R. A characterization of rare earth elements in coal ash generated during the utilization of Australian coals. *Int. J. Coal Prep. Util.* **2023**, *43*, 2106–2135. [CrossRef]

12. Reedy, R.C.; Scanlon, B.R.; Bagdonas, D.A.; Hower, J.C.; James, D.; Kyle, J.R.; Uhlman, K. Coal ash resources and potential for rare earth element production in the United States. *Int. J. Coal Sci. Technol.* **2024**, *11*, 74. [CrossRef]
13. Kuppusamy, V.K.; Holuszko, M. Sulfuric acid baking and water leaching of rare earth elements from coal tailings. *Fuel* **2022**, *319*, 123738. [CrossRef]
14. Honaker, R.Q.; Zhang, W.; Werner, J. Acid leaching of rare earth elements from coal and coal ash: Implications for using fluidized bed combustion to assist in the recovery of critical materials. *Energy Fuels* **2019**, *33*, 5971–5980. [CrossRef]
15. van Wyk, P.; Bradshaw, S.; Dorfling, C.; Ghosh, T.; Akdogan, G. Characterisation and hydrochloric acid leaching of rare earth elements in discard coal and coal fly ash. *Minerals* **2024**, *14*, 1070. [CrossRef]
16. Mokoena, K.; Mokhahlane, L.S.; Clarke, S. Effects of acid concentration on the recovery of rare earth elements from coal fly ash. *Int. J. Coal Geol.* **2022**, *259*, 104037. [CrossRef]
17. Chen, H.; Wen, Z.; Pan, J.; Zhang, L.; He, X.; Valeev, D.; Zhou, C. Study on leaching behavior differences of rare earth elements from coal fly ash during microwave-assisted HCl leaching. *Int. J. Coal Prep. Util.* **2023**, *43*, 1993–2015. [CrossRef]
18. Peiravi, M.; Ackah, L.; Guru, R.; Mohanty, M.; Liu, J.; Xu, B.; Zhu, X.; Chen, L. Chemical extraction of rare earth elements from coal ash. *Miner. Metall. Process.* **2017**, *34*, 170–177. [CrossRef]
19. Znamenackova, I.; Dolinska, S.; Hredzak, S.; Cablik, V.; Lovas, M.; Gesperova, D. Study of extraction of rare earth elements from hard coal fly ash. *Inżynieria Miner.* **2020**, *2*, 229–232. [CrossRef]
20. Ketegenov, T.; Kamunur, K.; Mussapyrova, L.; Batkal, A.; Nadirov, R. Enhancing Rare Earth Element Recovery from Coal Ash Using High-Voltage Electrical Pulses and Citric Acid Leaching. *Minerals* **2024**, *14*, 693. [CrossRef]
21. Banerjee, R.; Mohanty, A.; Chakravarty, S.; Chakladar, S.; Biswas, P. A single-step process to leach out rare earth elements from coal ash using organic carboxylic acids. *Hydrometallurgy* **2021**, *201*, 105575. [CrossRef]
22. Banerjee, R.; Chakladar, S.; Mohanty, A.; Chakravarty, S.; Chattopadhyay, S.K.; Jha, M.K. Review on the environment friendly leaching of rare earth elements from the secondary resources using organic acids. *Geosystem Eng.* **2022**, *25*, 95–115. [CrossRef]
23. Karan, R.; Sreenivas, T.; Kumar, M.A.; Singh, D.K. Recovery of rare earth elements from coal flyash using deep eutectic solvents as leachants and precipitating as oxalate or fluoride. *Hydrometallurgy* **2022**, *214*, 105952. [CrossRef]
24. Dodbiba, G.; Fujita, T. Trends in extraction of rare earth elements from coal ashes: A review. *Recycling* **2023**, *8*, 17. [CrossRef]
25. Tian, G.; Liu, H. Review on the mineral processing in ionic liquids and deep eutectic solvents. *Miner. Process. Extr. Metall. Rev.* **2024**, *45*, 130–153. [CrossRef]
26. Park, S.; Liang, Y. Bioleaching of trace elements and rare earth elements from coal fly ash. *Int. J. Coal Sci. Technol.* **2019**, *6*, 74–83. [CrossRef]
27. Ma, J.; Li, S.; Wang, J.; Jiang, S.; Panchal, B.; Sun, Y. Bioleaching rare earth elements from coal fly ash by *Aspergillus niger*. *Fuel* **2023**, *354*, 129387. [CrossRef]
28. Silva, R.G.; Morais, C.A.; Oliveira, É.D. Selective precipitation of rare earth from non-purified and purified sulfate liquors using sodium sulfate and disodium hydrogen phosphate. *Miner. Eng.* **2019**, *134*, 402–416. [CrossRef]
29. Masmoudi-Soussi, A.; Hammas-Nasri, I.; Horchani-Naifer, K.; Ferid, M. Rare earths recovery by fractional precipitation from a sulfuric leach liquor obtained after phosphogypsum processing. *Hydrometallurgy* **2020**, *191*, 105253. [CrossRef]
30. Xing, M.; Wu, X.; Li, Z.; Zhang, F.; Wang, Y.; Zhao, L. Rare earth element recovery and aluminum-rich residue production from high alumina fly ash by alkali pre-desilication enhance the mechanochemical extraction process. *Process Saf. Environ. Prot.* **2023**, *175*, 60–69. [CrossRef]
31. Praneeth, S.; Sakr, A.K.; Dardona, M.; Tummala, C.M.; Roy, P.K.; Dittrich, T.M. Selective separation and recovery of rare-earth elements (REEs) from acidic solutions and coal fly ash leachate by novel TODGA-Impregnated organosilica media. *Chem. Eng. J.* **2024**, *500*, 156849. [CrossRef]
32. Hassas, B.V.; Rezaee, M. Selective precipitation of rare earth and critical elements from acid mine drainage-Part II: Mechanistic effect of ligands in staged precipitation process. *Resour. Conserv. Recycl.* **2023**, *188*, 106655. [CrossRef]
33. Liu, P.; Zhao, S.; Xie, N.; Yang, L.; Wang, Q.; Wen, Y.; Chen, H.; Tang, Y. Green approach for rare earth element (REE) recovery from coal fly ash. *Environ. Sci. Technol.* **2023**, *57*, 5414–5423. [CrossRef]
34. Farrah, H.E.; Lawrance, G.A.; Wanless, E.J. Solubility of calcium sulfate salts in acidic manganese sulfate solutions from 30 to 105 °C. *Hydrometallurgy* **2007**, *86*, 13–21. [CrossRef]
35. Firsching, F.H.; Brune, S.N. Solubility products of the trivalent rare-earth phosphates. *J. Chem. Eng. Data* **1991**, *36*, 93–95. [CrossRef]
36. Cetiner, Z.S.; Wood, S.A.; Gammons, C.H. The aqueous geochemistry of the rare earth elements. Part XIV. The solubility of rare earth element phosphates from 23 to 150 °C. *Chem. Geol.* **2005**, *217*, 147–169. [CrossRef]
37. Gausse, C.; Szenknect, S.; Qin, D.W.; Mesbah, A.; Clavier, N.; Neumeier, S.; Bosbach, D.; Dacheux, N. Determination of the solubility of rhabdophanes $LnPO_4 \cdot 0.667H_2O$ (Ln = La to Dy). *Eur. J. Inorg. Chem.* **2016**, *2016*, 4615–4630. [CrossRef]
38. Stefánsson, A. Iron (III) hydrolysis and solubility at 25 °C. *Environ. Sci. Technol.* **2007**, *41*, 6117–6123. [CrossRef]

39. Zou, Y.; Chernyaev, A.; Seisko, S.; Sainio, J.; Lundström, M. Removal of iron and aluminum from hydrometallurgical NMC-LFP recycling process through precipitation. *Miner. Eng.* **2024**, *218*, 109037. [CrossRef]
40. Destefani, T.A.; Onaga, G.L.; de Farias, M.A.; Percebom, A.M.; Sabadini, E. Stabilization of spherical nanoparticles of iron (III) hydroxides in aqueous solution by wormlike micelles. *J. Colloid Interface Sci.* **2018**, *513*, 527–535. [CrossRef]
41. De Hek, H.; Stol, R.J.; De Bruyn, P.L. Hydrolysis-precipitation studies of aluminum (III) solutions. 3. The role of the sulfate ion. *J. Colloid Interface Sci.* **1978**, *64*, 72–89. [CrossRef]
42. Jadhav, S.V.; Gadipelly, C.R.; Marathe, K.V.; Rathod, V.K. Treatment of fluoride concentrates from membrane unit using salt solutions. *J. Water Process Eng.* **2014**, *2*, 31–36. [CrossRef]
43. Senevirathna, H.L.; Lee, W.C.; Wu, S.; Bai, K.; Wu, P. Transforming desalination brine into highly reactive magnesium oxide and life cycle analysis. *Watershed Ecol. Environ.* **2025**, *7*, 36–46. [CrossRef]
44. Beltrami, D.; Deblonde, G.J.P.; Bélair, S.; Weigel, V. Recovery of yttrium and lanthanides from sulfate solutions with high concentration of iron and low rare earth content. *Hydrometallurgy* **2015**, *157*, 356–362. [CrossRef]